# New perspectives by imaging modalities for an old illness: Rheumatic mitral stenosis

*Tuğba Kemaloğlu Öz[#]*,  *Özge Özden Tok[1, #]*,  *Leyla Elif Sade[2]*

Department of Cardiology, İstinye University, Liv Hospital Ulus; İstanbul-*Turkey*
[1]Department of Cardiology, Memorial Bahçelievler Hospital; İstanbul-*Turkey*
[2]Department of Cardiology, Faculty of Medicine, Başkent University; Ankara-*Turkey*

## ABSTRACT

Mitral stenosis (MS) is a progressive and devastating disease and most often occurs among young women. Given its considerable prevalence in Mediterranean and Eastern European countries according to the Euro Heart Survey, new imaging modalities are warranted to improve the management of patients with this condition. A wide spectrum of abnormalities occurs involving all parts of this complex structure and causing different grades of MS and/or regurgitation as a consequence of rheumatic affection. Novel imaging modalities significantly improved the assessment of several aspects of this rheumatic destructive process including the morphological alterations of the mitral valve (MV) apparatus, left atrial (LA) function, LA appendage, right and left ventricular (LV) functions, and complications, namely, atrial fibrillation and thromboembolic events. Furthermore, new imaging modalities improved the prediction of outcome of patients who underwent percutaneous balloon mitral comissurotomy and changed the paradigm of patient selection for intervention and risk stratification. The present review aimed to summarize the role of new multimodality, multiparametric imaging approaches to assess the morphological characteristics of the rheumatic MS and its associated complications, and to guide patient management. *(Anatol J Cardiol 2020; 23: 128-40)*
**Keywords:** mitral stenosis, rheumatic heart disease, echocardiography, 3-D echocardiography, strain, multimodality imaging

## Introduction

Rheumatic fever is the most important cause of mitral valve (MV) disease in low-income countries (1, 2); the prevalence of mitral stenosis (MS) remains high in Mediterranean and Eastern European countries according to the Euro Heart Survey, accounting for 12% of valvular diseases in Europe (3). The importance of this irreversible, progressive disease is severalfold: It usually affects young women, is a threat among women of childbearing age, and is associated with 1%–6% annual risk of thromboembolic events (4). MV has a complex structure with saddle shape annulus, two leaflets with six scallops, comissures, and two papillary muscles attached to both leaflets by numerous cordae tedineae. A wide spectrum of abnormalities occurs involving all parts of this complex structure and causing different grades of MS and/or regurgitation as a consequence of rheumatic affection. Novel imaging modalities significantly improved

the assessment of several aspects of this rheumatic destructive process. The present review aimed to summarize the role of new multimodality, multiparametric imaging approaches to assess the morphological characteristics of rheumatic MS and its associated complications, and to guide patient management.

### Morphological features

The hallmark of rhematic MS is commissural fusion. Involvement of subvalvular apparatus with chordal fusion, thickening, and further shortening restricts mobility and increases rigidity of the leaflets. In the later stages of the disease, varying degrees of superimposed calcification worsens leaflet motion. The disease typically progresses from the commissures and the tips of the leaflets to the more proximal parts (body and base) and to the subvalvular apparatus (Fig. 1, Videos 1a-1c).

In degenerative MS, which occurs in older adults, the main mechanism is heavy calcification that starts from the annulus

Anatol J Cardiol 2020; 23: 128-40
DOI:10.14744/AnatolJCardiol.2020.01575

Kemaloğlu Öz et al.
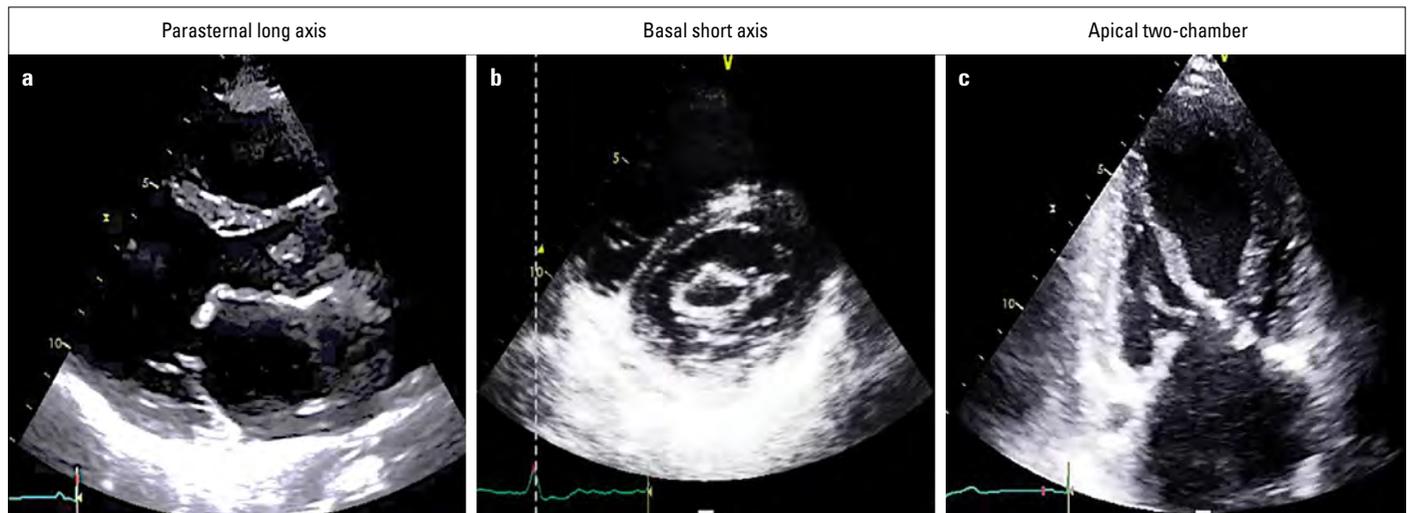Multimodality imaging for mitral stenosis  *129*

**Figure 1.** (a–c) Typical features of rheumatic mitral stenosis by 2D transthoracic echocardiography. (a, b) Commissural fusion, leaflet thickening and rigidity and (c) involvement of subvalvular apparatus with chordal fusion, thickening, and shortening (Videos 1a–c)

and extends toward the bases of the leaflets mostly affecting the posterior leaflet. In the absence of extreme leaflet calcification and thickening, annular calcification alone does not lead to severe hemodynamic consequences because the basal parts of the leaflets are affected more than the tips without commissural fusion (Fig. 2, Video 2).

Radiation-induced MS is a rare clinical condition. It is characterized by fibrosis and calcification of the valve usually extending from the anterior leaflet into the mitral-aortic fibrosa without commissural fusion. The posterior leaflet can be involved as well (Fig. 3, Videos 3a, 3b). After a long latent period following radiation exposure, significant valve dysfunction occurs in 1% of patients with radiation-induced MS at 10 years, in 4% at 15 years, and in 6% at 20 years (5).

Congenital MS is extremely rare and is characterized by supra- or subvalvular rings, annular hypoplasia, double orifice mitral valve (MV), hypoplastic papillary muscle, and parachute

MV. Calcification does not usually occur in the valvular or subvalvular apparatus (Fig. 4, Videos 4a-4c) (6).

### Assessment of rheumatic MS by 2D and Doppler echocardiography

Classically, the morphological characteristics of the MV can be defined by 2-D echocardiography (2DE) and the mitral valve area (MVA) by 2D planimetry and Doppler evaluation. These methods have several well-known limitations. Doppler evaluations based on mean and peak gradients and pressure half-time are affected by hemodynamic conditions including heart rate, transmitral flow volume, left ventricular (LV), and left atrial (LA) compliances (7). Within the first 48–72 hours following percutenous balloon mitral commissurotomy (PBMC), pressure half-time and Gorlin calculations are unreliable due to the abrupt changes in mitral gradient and LA compliance. Although the assessment of MVA by 2D planimetry is not influenced by hemodynamic changes, determining
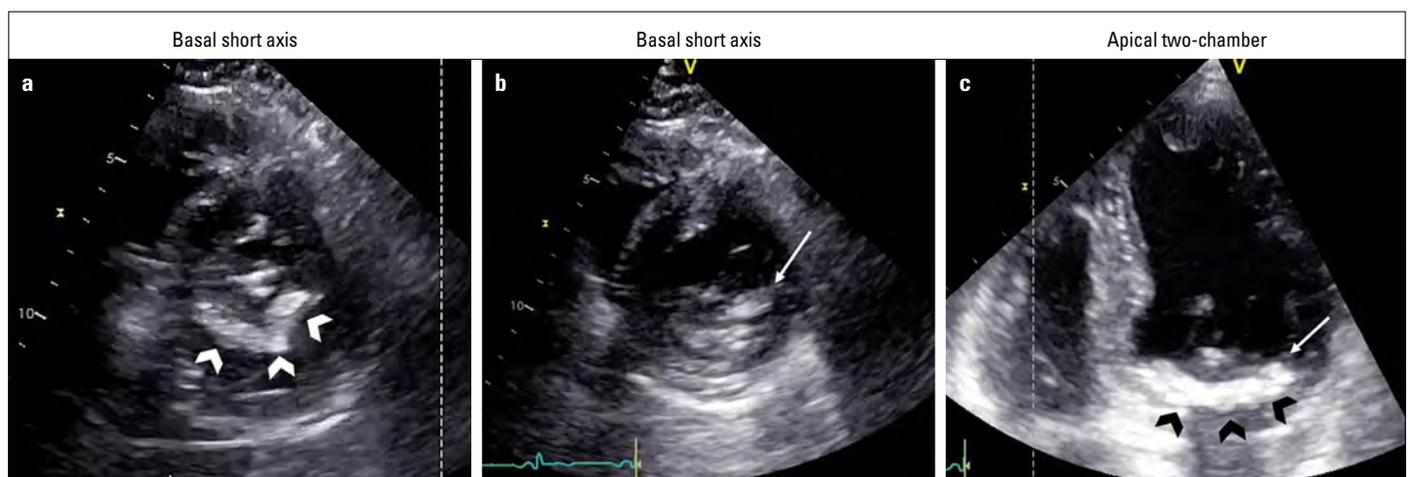


**Figure 2.** (a) Degenerative calcific MV. Note that the calcification mainly involves the annulus (arrow heads) extending toward the body of the leaflets. (b, c) The tips of the leaflets are relatively spared, (arrow) in contrast to rheumatic mitral stenosis, in which the calcification and thickening starts from the tips of the leaflets (Video 2)
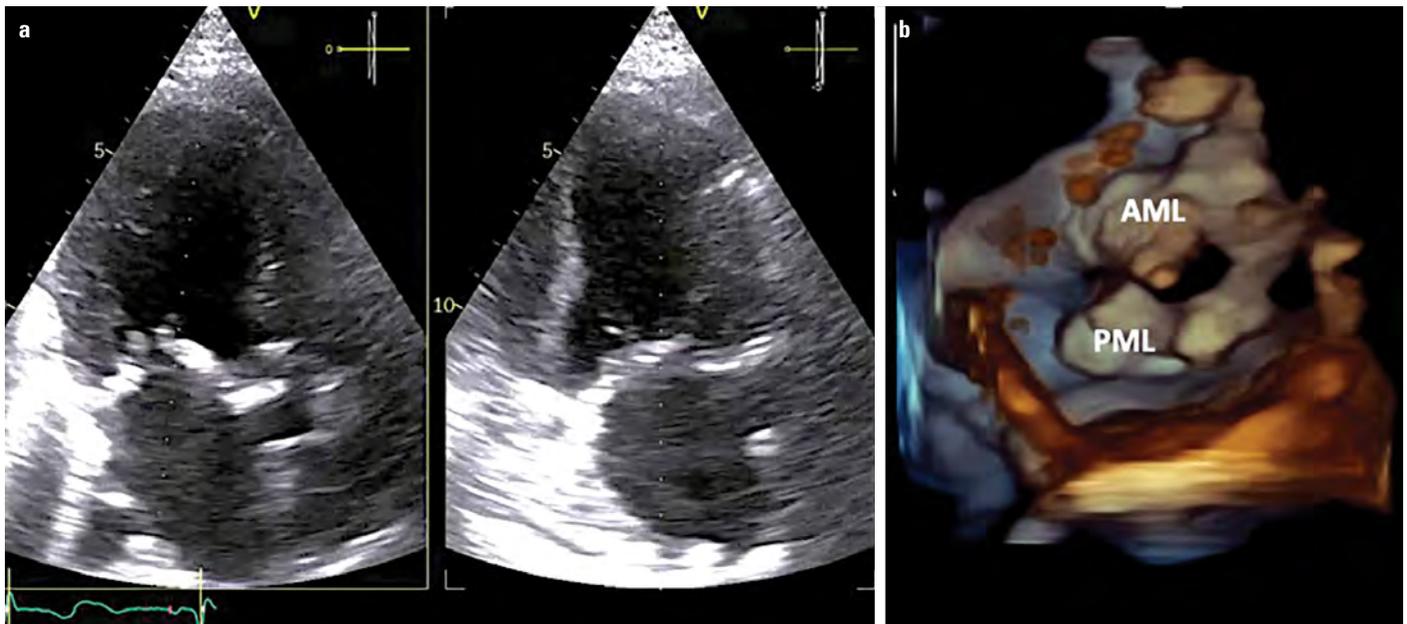
**130** Kemaloğlu Öz et al.
Multimodality imaging for mitral stenosis

Anatol J Cardiol 2020; 23: 128-40
DOI:10.14744/AnatolJCardiol.2020.01575



**Figure 3.** Radiation-induced mitral stenosis in (a) biplane orthogonal long axis views and (b) 3D volume rendered image from the ventricular perspective. AML - anterior mitral leaflet, PML - posterior mitral leaflet (Videos 3a, 3b) (Courtesy of Dr. Ruxandra Jurcut)
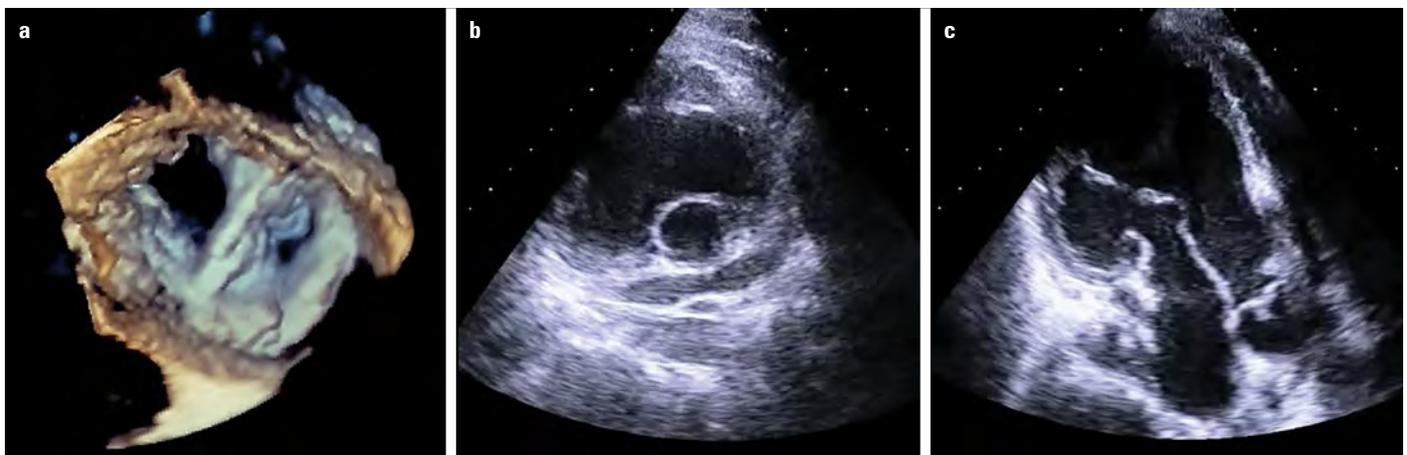


**Figure 4.** Congenital mitral stenosis. (a) 3D rendered display of double orifice MV from LA perspective, (b) parachute MV from parasternal short axis, and (c) apical long axis views (Videos 4a–4c)

the correct orifice cut plane from the LV short-axis view is difficult due to funnel-shaped narrowing (Fig. 5). Proximal isovelocity surface area (PISA) method is technically more demanding and recommended only if pressure half-time and planimetry are inconclusive (8). PISA method assumes that the flow convergeance zone is hemispheric on the atrial side, which is not true for MS due to the limited opening angle of the leaflets (9). PISA method requires angle correction for the evaluation of MS, complicating its use. The use of continuity equation assuming that the transmitral flow is equal to the aortic stroke volume is cumbersome and only valid in the absence of significant valvular regurgitations (8).

### Assessment of rheumatic MS by three-dimensional (3D) echocardiography

3-D echocardiography (3DE) allows detailed and accurate morphological analysis of the entire MV including the leaflets, commissures, annulus, and subvalvular apparatus. Commissural fusion is visualized by 3DE with more precision than 2DE (10), although calcifications are better characterized by 2DE (Fig. 6, Videos 5a, 5b). En face views of MV from either LA or LV perspectives are easily obtained. Both transthoracic and transoesophageal (TOE) 3DE provide optimally oriented en face view of the stenotic orifice for planimetric measurement (Fig. 7, Videos 6a-6c) (11). This measurement provides the anatomic valve area, which is slightly higher than the Doppler-derived effective orifice area at the vena contracta level (12). Excellent intra- and interobserver correlations and higher interobserver agreement were found with 3D TOE measurements of MVA (13). 3DE facilitates communication with the operators. Yet, poor acoustic window, severe calcifications of the leaflet tips, inadequate gain settings, and technical expertise of the echocardiographer remain as limitations for planimetric evaluation of MVA by 3DE.
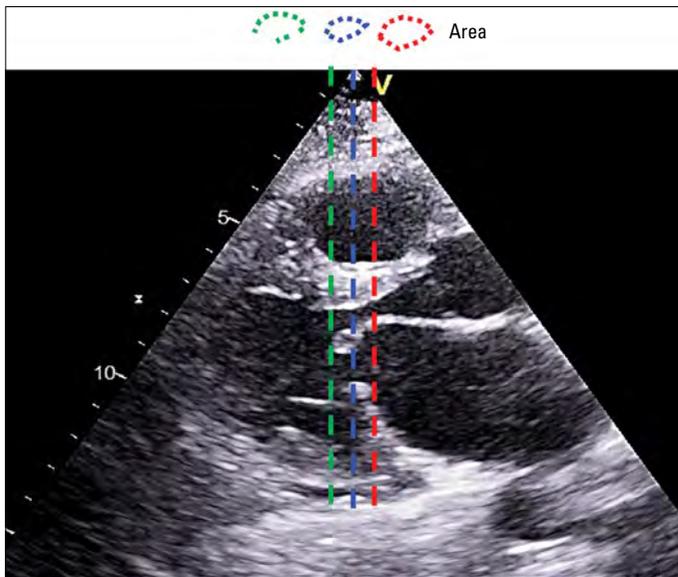
Anatol J Cardiol 2020; 23: 128-40
DOI:10.14744/AnatolJCardiol.2020.01575

Kemaloğlu Öz et al.
Multimodality imaging for mitral stenosis *131*

**Figure 5.** Imprecise stenotic MVA depending on the 2D transverse cut plane due to a funnel-shaped stenotic orifice

The calculation of the valve area of degenerative calcific MS is more challenging. The MV orifice is irregular, and the narrowest portion is not located at the tips of the leaflets but at the basal region. Therefore, selection of an accurate plane is more difficult than rheumatic MS and makes the use of 3DE crucial (14).

### Associated pathologies with MS
### Left atrial remodeling

LA dilatation reflects the hemodynamic burden of MS and is of prognostic importance. LA volume is independently associated with an increased risk for embolic cerebrovascular disease (15) and the development of atrial fibrillation (16), which play a key role in patient management. Linear measurements of the
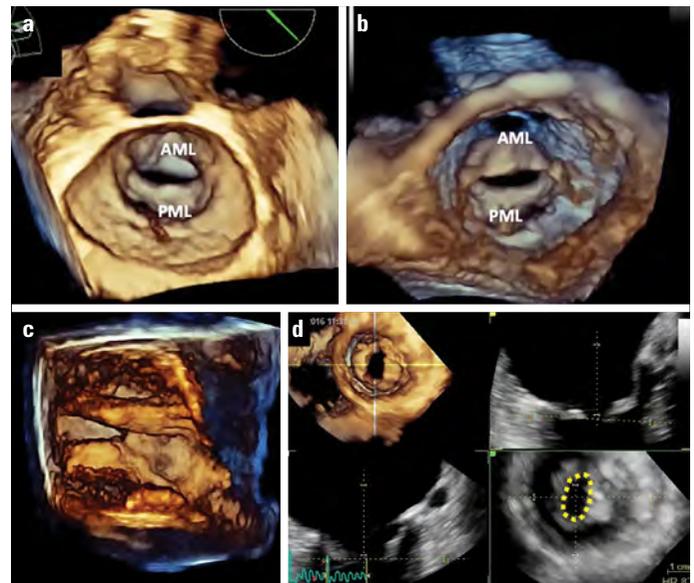


**Figure 7.** Stenotic MV (a) from the LA surgeon's view, (b) from the ventricular perspective, (c) 3D parasternal long axis cut plane showing chordal thickening and fusion, and (d) flexislice from 3D dataset to obtain the optimal en face view of the MVA for measurement by planimetry (Videos 6a-6c)

AML - anterior mitral leaflet, PML - posterior mitral leaflet

LA are outdated and insufficient because of the asymmetrical enlargement of the LA (17). LV and LA axes are not aligned. LA dilatation should be quantified using volumetric methods such as the modified Simpson's biplane method of discs from LA focused views or by 3DE.

LA volumes derived from 2DE are typically smaller than the volumes derived from multidetector computed tomography (MDCT) or cardiac magnetic resonance (CMR) (18, 19). However, real-time 3DE measurements of LA volumes have been validated
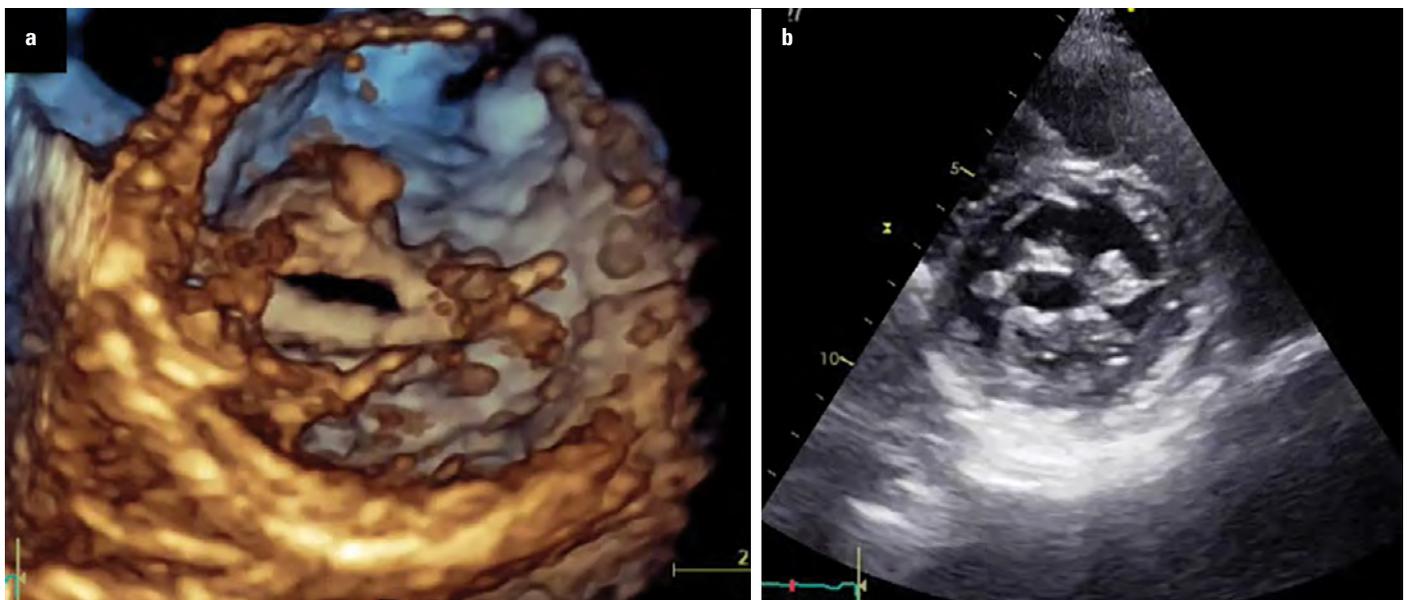


**Figure 6.** Commissural (a) fusion and (b) calcification by 2DE versus 3DE. Note that commissural fusion is more precisely appreciated by 3DE; however, calcifications are more easily appreciated by 2DE (Videos 5a, 5b)

*132* Kemaloğlu Öz et al.
Multimodality imaging for mitral stenosis

Anatol J Cardiol 2020; 23: 128-40
DOI:10.14744/AnatolJCardiol.2020.01575

against MDCT and CMR (20, 21) and are more accurate and re-producible than 2DE (19). LA phasic function can be assessed by means of volume changes over the cardiac cycle or strain and strain rate by quantifying LA reservoir, conduit, and booster pump functions (Fig. 8, 9). Early alterations in LA phasic function can increase the hemodynamic burden and risk imposed by MS. The LA function deteriorates before an overt LA dilatation occurs (22). LA remodeling also includes interstitial fibrosis, which correlates with LA dilatation, and decreases LA reservoir function (23). Such structural and functional changes of the LA can lead to a reduction in LA flow dynamics and blood stagnation and trigger atrial fibrillation and thrombus formation (16, 24, 25).

### Left atrial appendage morphology and function

LA enlargement in association with MS causes blood stasis and thrombus formation not only in the LA but also in the LA appendage (26). In those with rheumatic MS, thrombi develop more frequently in patients with LA than in those with nonvalvular atrial fibrillation. LA appendage is best visualized with TOE to exclude thrombus upon suspicion or before PMBC. Although 3DE is sometimes helpful in diagnosing thrombus, it cannot provide a precise description of the tissue properties and is not reliable for differentiating pectinate muscles from thrombi. The most valuable approach is to use multiplane images extracted from the 3D TOE dataset. This approach allows visualization of all parts of an irregular appendage (Fig. 10). If the spontaneous echocontrast in the LA appendage is extremely dense, it may obscure a threatening thrombus. In such instances, contrast agents or MDCT should be used to exclude thrombus (27).

3D TOE is also crucial for the assessment of the LA appendage orifice with clear delineation of its shape, dimensions, and surrounding structures like pulmonary vein, MV, and circumflex artery whenever LA appendage occlusion is planned (Fig. 11).

### Left ventricular dysfunction

LV dysfunction occurs in patients with MS due to the chronic reduction in preload (28). Even with preserved EF, subclinical LV systolic dysfunction can be detected by strain imaging and 3D methods (29). Favorable changes after successful PBMC can also be tracked by strain imaging, which can accurately determine a reduction in LV diastolic filling rather than irreversible structural abnormality and can help decrease LV mechanical performance in patients with severe MS (Fig. 12) (30).

### Tricuspid valve (TV) dysfunction and right ventricular (RV) dilatation

Severe MS can lead to secondary pulmonary hypertension (PHT). Long-standing PHT causes tricuspid annular dilatation
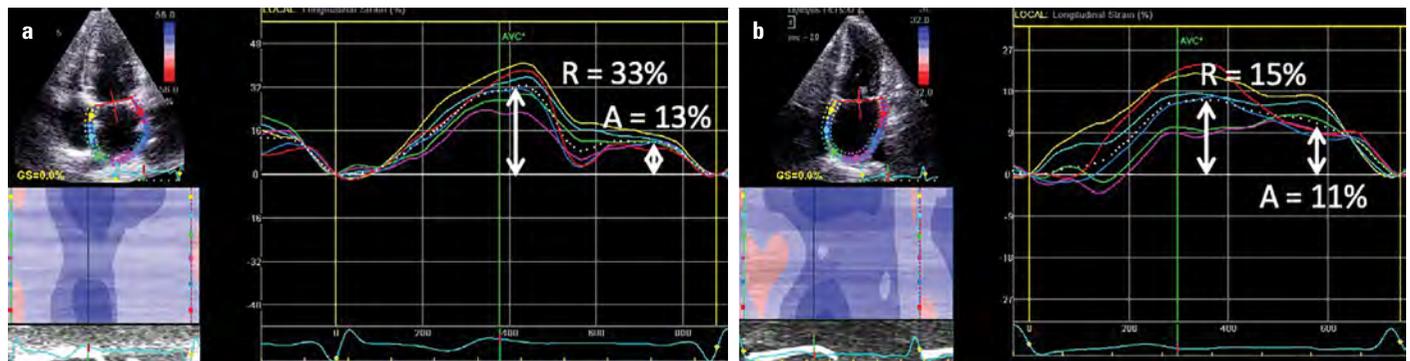


**Figure 8.** LA phasic function by 2D speckle tracking strain. (a) Normal and (b) LA dysfunction in a patient with stenotic MV.
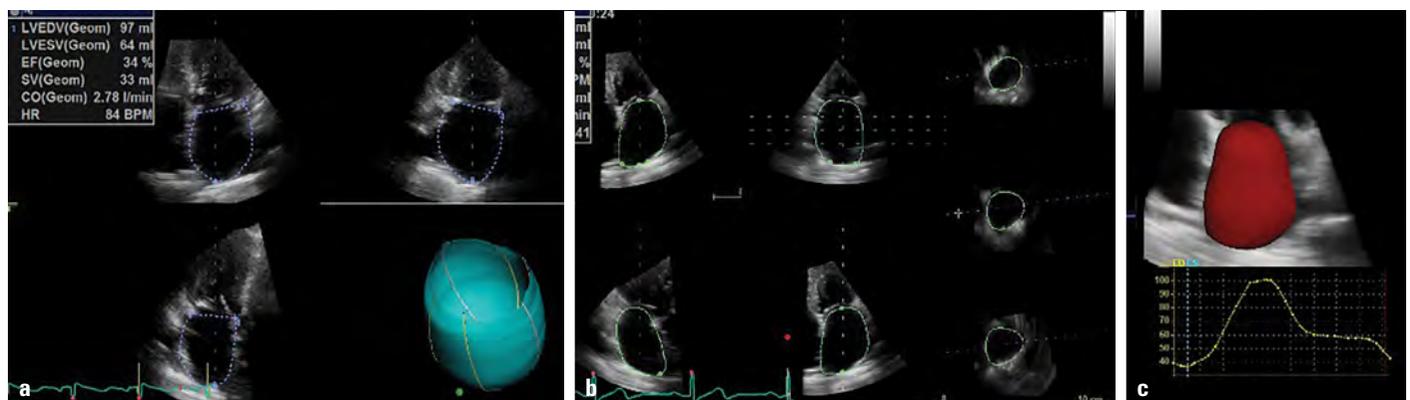R - reservoir; A - booster pump function



**Figure 9.** LA volume and ejection fraction by 3DE. (a) Measurement by triplane, (b) measurement by 3D full volume, and (c) volume rendered image of the LA and the corresponding time-volume curve showing phasic function
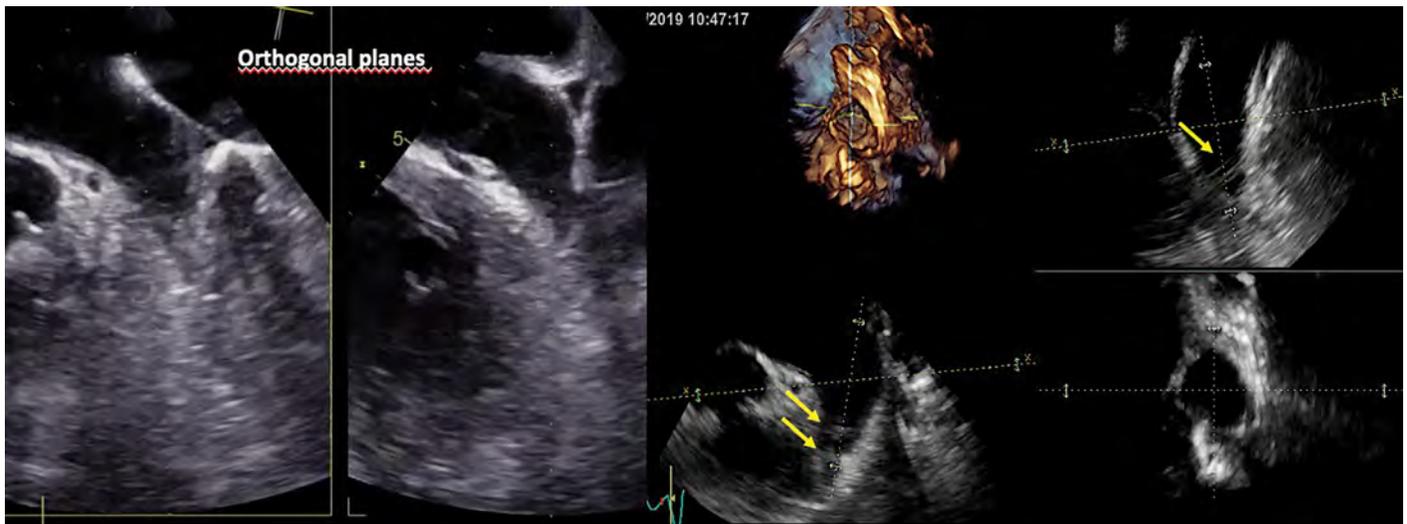
Anatol J Cardiol 2020; 23: 128-40
DOI:10.14744/AnatolJCardiol.2020.01575

Kemaloğlu Öz et al.
Multimodality imaging for mitral stenosis   *133*

**Figure 10.** LA appendage by 3D TOE. Note the thrombus captured on the flexislice display (arrow), which was not visible on conventional cut planes
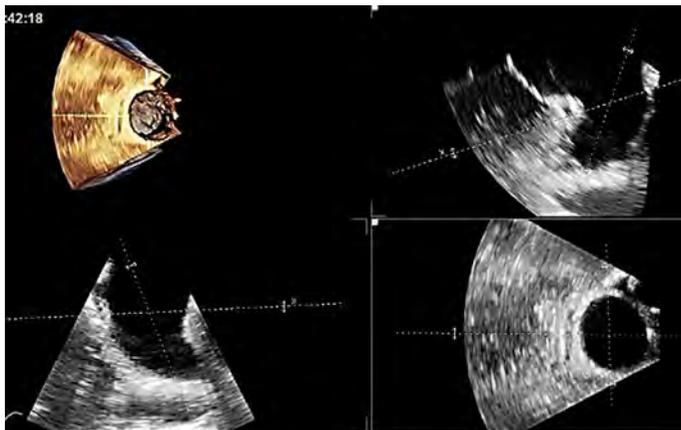


**Figure 11.** Optimal en face view of LA appendage orifice on 3D volume rendered display and correct measurement planes by flexislice

and right ventricular (RV) remodeling, which in turn beget tricuspid regurgitation (TR) by causing papillary muscle displacement and tethering of the tricuspid valve (TV) leaflets (Fig. 13a-13d, Video 7) (31). In patients with rheumatic MS, TR is usually secondary to PHT. TV is rarely affected by the rheumatic process. However, multivalvular rheumatic process may occur and should be carefully described and quantified to optimize the patient outcome. Commissural fusion, leaflet thickening, and chordae thickening and fusion can be visualized to confirm the rheumatic process affecting the TV, even more frequently than previously thought by means of 3DE (Fig. 14, Video 8). 3DE can be used for quantifying the stenotic TV area by direct planimetry from an optimally oriented perpendicular cut plane obtained by multiplanar reconstruction (Fig. 14).

By contrast, functional TR requires a comprehensive assessment of tricuspid annulus, papillary muscle displacement, leaflet tethering, tenting, and RV remodeling. Tricuspid annular dilatation, as measured by 2DE from the apical four-chamber view in everyday clinical practice, does not quantify the correct dilatation that typically occurs from the anteroseptal commissure to the anterolateral commissure. With 3DE, one can correctly quantify the tricuspid annular dilatation from the surgical view (Fig. 13b). Diagnosis of rheumatic TV involvement and correct measurement of the tricuspid annular dilatation are both important to guide the surgeons and to plan timely interventions addressing the underlying TV pathology in order to prevent clinical deterioration during follow up, because many of these patients develop severe TV dysfunction and intractable right heart failure despite the normal functioning of mitral prostheses later in the disease course.
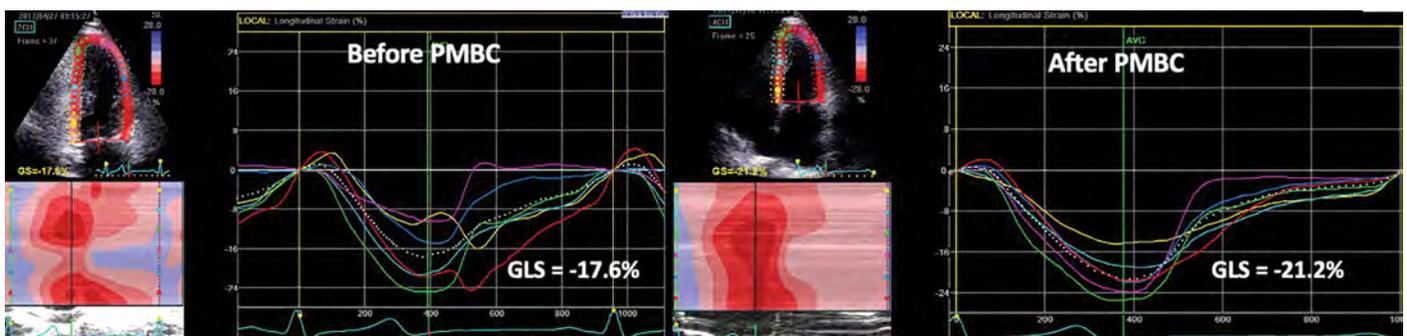


**Figure 12.** LV function by longitudinal strain before and after percutaneous balloon mitral commissurotomy. Note the improvement in strain from −17.6% to −21.2% despite normal ejection fraction before and after the procedure

*134* Kemaloğlu Öz et al.
Multimodality imaging for mitral stenosis

Anatol J Cardiol 2020; 23: 128-40
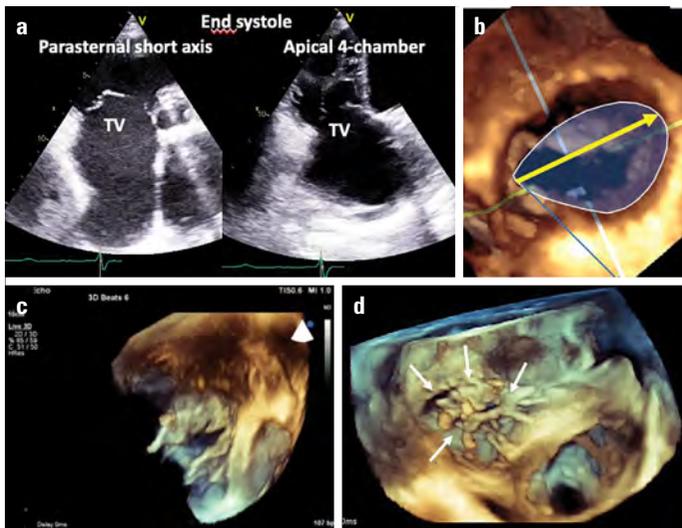DOI:10.14744/AnatolJCardiol.2020.01575

**Figure 13.** Functional TR. (a) Tenting of the leaflets and dilatation of the tricuspid annulus by 2D and (b) annular dilatation from surgical perspective by 3DE with correct measurement of annular dilatation in surgical view (yellow arrow). (c) Tenting of tricuspid leaflets and (d) chordal tethering (arrows) from the ventricular perspective by 3DE (Video 7) (c and d, courtesy of Dr. Omaç Tüfekçioğlu)
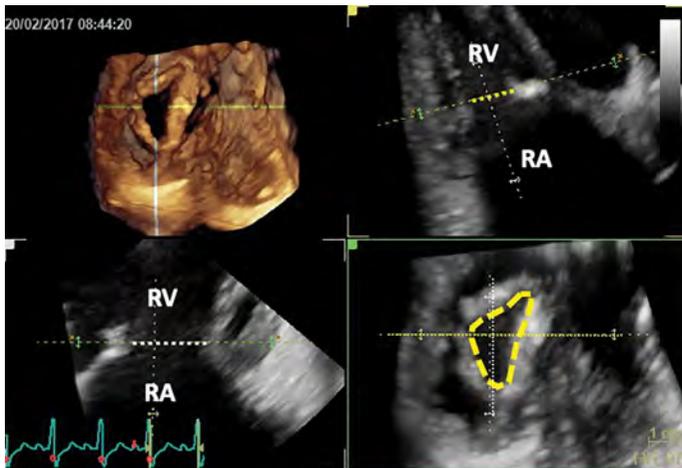
TV - tricuspid valve



**Figure 14.** Rheumatic tricuspid stenosis with commissural fusion, rigid septal leaflet, and thickening of all three leaflets particularly at the tips as viewed from transthoracic apical window. Note that the optimal orientation of stenotic TV orifice by multiplanar 3D images enables planimetric quantification of TV area (yellow dashed line) (Video 8)

RV dilatation is best assessed by 3D volume quantification due to the peculiar shape of this chamber wrapping around the LV. The assessment of RV volumes by 3DE has been tested against CMR. 3DE tends to underestimate RV volumes compared with CMR. However, its reproducibility was validated and serves as an accurate means of assessing RV volumes and functions (32). Subclinical RV dysfunction occurs in the early stages of MS and can be detected by strain quantification at rest (33). Quantification of RV dysfunction, before significant dilatation occurs, has potential implications for patient management as it is not a simple bystander of MS but reflects the

hemodynamic burden and impacts the prognosis of patients with rheumatic MS (34).

### Role of transosophageal echocardiography

The use of TOE is recommended for the assessment of MS in patients with poor transthoracic acoustic windows, for pre-procedural assessment of MV morphology before PBMC, and to rule out thrombi in the LA and/or LA appendage (35). TOE with or without 3DE is definitely superior to transthoracic echocardiography in terms of visualizing morphological abnormalities. 3D TOE allows excellent evaluation of commissural fusion and MVA by planimetry (Fig. 7) (36).

3D TOE is useful in visualizing the full delineation of LA appendage and interatrial septum morphology for planning PBMC. Guidance of PMBC by 3D TOE secures and facilitates safe transseptal puncture, helps to orient the balloon to the stenotic orifice, and decreases or even prevents radiation exposure during the procedure, which is very important considering the patients' young age and female gender preponderance with possible late diagnoses during pregnancy (Fig. 15) (37, 38).

### Role of stress echocardiography

In some patients, symptoms may be discordant with the severity of MS. Stress echocardiography is mainly useful for (1) asymptomatic patients with echocardiography findings of severe MS or (2) symptomatic patients with echocardiography findings of mild or moderate MS. Stress echocardiography helps evaluate the true hemodynamic burden of MS. The estimation of pulmonary artery pressure during stress echocardiography (exercise or dobutamine) helps clinicians decide whether other types of interventions or medical therapy should be provided (35, 39, 40). As the heart rate increases with exercise, the diastolic transmitral gradient increases exponentially as well as the LA pressure; consequently, pulmonary capillary wedge pressure increases due to the fixed stenotic mitral orifice. Exercise stress echocardiography (preferentially supine bicycle) is more conclusive from a pathophysiologic standpoint than pharmacological stress echocardiography for the assessment of MS severity and its hemodynamic burden; it is the preferred modality and uncovers symptoms in almost 50% of patients with moderate-to-severe MS who are asymptomatic at rest (41). Dobutamine stress echocardiography is an alternative only if the patient is unable to perform exercise (40). If the MV morphology is suitable for PBMC procedure, patients without symptoms but with objective significant limitation on exercise may be considered for PBMC (40). PBMC can be considered in patients with a valve area of more than 1.5 cm$^2$ who show a transmitral mean gradient of >15 mm Hg, pulmonary artery wedge pressure of ≥25 mm Hg, or pulmonary artery systolic pressure of >60 mm Hg during exercise (35). When a dobutamine stress test is performed, the evaluation of pulmonary pressure is not helpful. A mean transmitral gradient more than 18 mm Hg during the stress test shows the high probability of clinical deterioration or the need for surgery (42).

Anatol J Cardiol 2020; 23: 128-40
DOI:10.14744/AnatolJCardiol.2020.01575

Kemaloğlu Öz et al.
Multimodality imaging for mitral stenosis 135

**Figure 15.** Percutaneous balloon mitral commissurotomy in a pregnant woman with minimal fluoroscopy, thanks to 3D TOE guidance (Asterix: Innoue Balloon from the atrial perspective oriented to the stenotic mitral orifice)

### Echocardiography for percutaneous mitral balloon commissurotomy

The major goal of PBMC is to achieve a complete bilateral commissural opening. Therefore, commissural fusion is a prerequisite for PBMC. Wilkins score has been the most widely used scoring system until recently to assess the anatomical suitability of the valve for PBMC (43). Wilkins score takes into account leaflet mobility, thickness, calcification, and involvement of subvalvular apparatus; it is used to grade each of these components from 1 to 4. From each of the components of the Wilkins score system, valvular thickening has the highest correlation with changes in MV area. An echo score of less than 8 is associated with lower rates of restenosis and better survival from redo PBMC and MV replacement. However, patients with a score of more more than 12 are less likely to have a satisfactory result and are referred for surgery. Patients with an echo score ranging from 8 to 12 need more detailed morphological and clinical evaluation (44). Despite a significant negative correlation between the absolute change in MV area achieved after PBMC and the total echo score, the relationship is scattered and the score remains relatively imprecise for predicting the final result from PBMC. Approximately 40% of patients with an echo score of more than 8 demonstrated a good outcome (45). Wilkins score has additional limitations: lack of precise delineation of commissural involvement, localization of calcium deposition (valvular or commissural), uneven distribution of pathologic abnormalities, discrimination of relative contribution of each variable (no weighting of variables), and lack of inclusion of TOE and 3DE findings. These morphological parameters impact the success of PBMC (46). PBMC is unlikely to increase the MV area if commissural fusion is absent or the commissures resist splitting due to the presence of calcification (Fig. 16). Not only the extent of calcification, but also the localization of calcification at the commissures, uneven distribution of commissural fusion, and irregular distribution of calcification on the leaflets are important for the success of PBMC (46-48). Because irregular calcifications

may cause tears on the leaflet, the instability of the balloon during inflation and asymmetrical commissural involvement may result in excessive splitting of the less or noncalcified commissure. Patients with low Wilkins score but unfavorable calcifications have significantly lower rates of success; however, a high Wilkins score does not preclude the possibility of a satisfactory result. PBMC can be an option if there is no commissural calcification, despite relatively high Wilkins scores (47, 49).

Consequently, other scoring systems have been proposed to improve patient selection for PBMC. Cormier score divides the patients into three groups depending on leaflet mobility, calcification, and affection of subvalvular apparatus: group 1, pliable leaflets and mild chordal thickening (chordae >10 mm long); group 2, pliable mitral leaflets and extensive subvalvular disease (thickened chordae <10 mm); and group 3, calcified valves confirmed by fluoroscopy (50). Many other 2DE scoring systems have been proposed, but none of them was shown to be superior to other scoring systems except Nune's and Anwar's scoring systems (51, 52).

In Nune's scoring system (51), the quantification is based on the assessment of commissural (a)symmetry as the ratio of leaflet area on either side of the minor dimension of the valve in the short-axis view and the leaflet displacement by measuring the maximum apical displacement of the leaflets relative to the annulus in the apical four-chamber view in addition to the assessment of subvalvular involvement (Fig. 17): MVA $\leq 1$ cm$^2$ is assigned 2 points, maximum displacement of leaflets $\leq 12$ mm is assigned 3 points, commissural area ratio $\geq 1.25$ is assigned 3 points, and finally subvalvular involvement 3 points. Three risk groups are defined based on the following scores: 0–3 (low), 4–5 (intermediate), and 6–11 (high) and with observed suboptimal PBMC results of 16.9%, 56.3%, and 73.8%, respectively. A net reclassification improvement of 45% over Wilkins score has been reported with this scoring system, which was found particularly valuable in patients who were in the intermediate-risk group (score, 8–12) by Wilkins score.
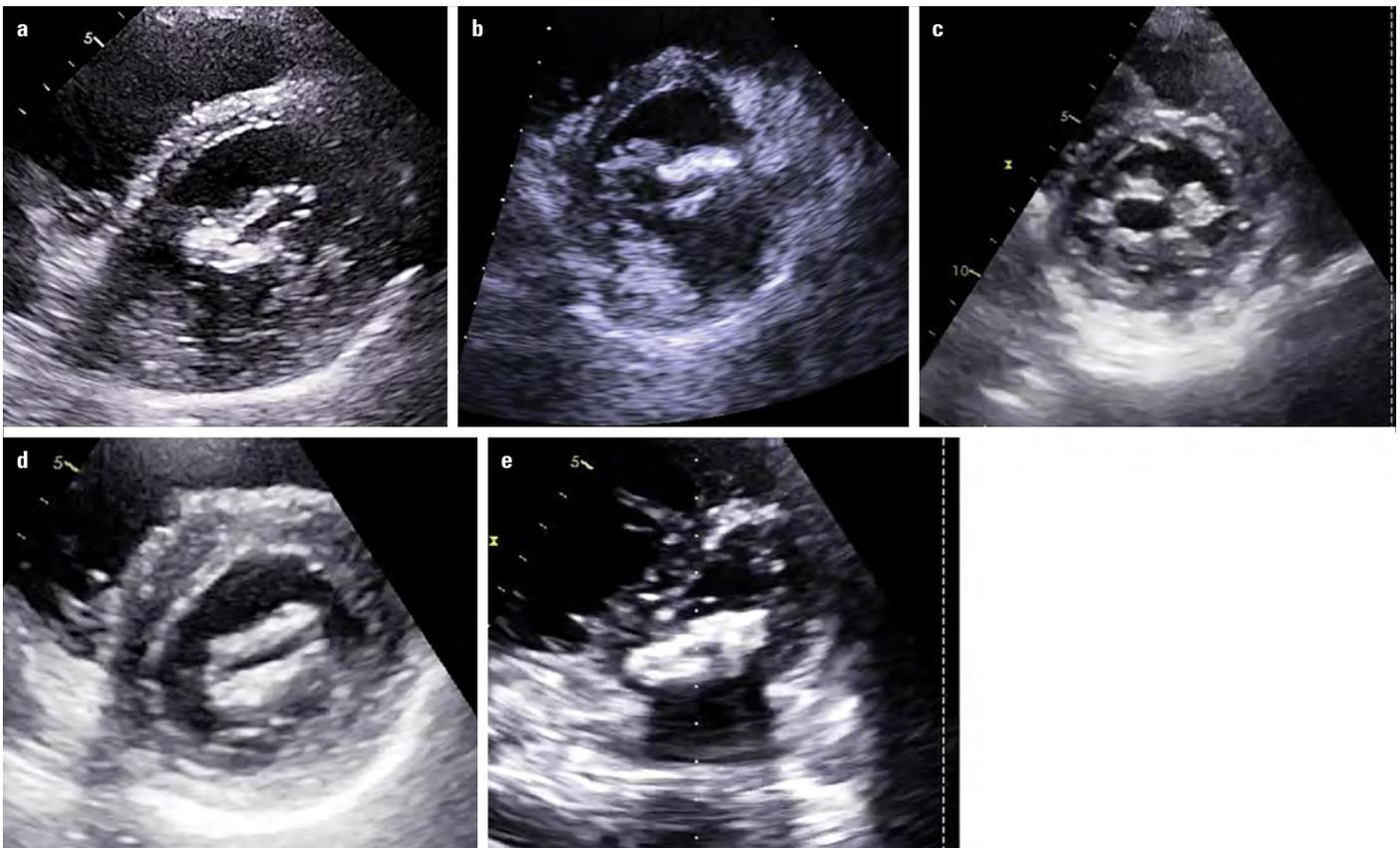
*136* Kemaloğlu Öz et al.
Multimodality imaging for mitral stenosis

Anatol J Cardiol 2020; 23: 128-40
DOI:10.14744/AnatolJCardiol.2020.01575

**Figure 16.** Calcification patterns: (a, b) Asymmetric commissural calcification, (c) asymmetrical bi-commissural and irregular leaflet calcification, (d) diffuse leaflet calcification with commissural sparing, and (e) diffuse severe calcification of leaflets and commissures



$$\text{Symmetry} = \frac{\text{Area max}}{\text{Area min}}$$

**Figure 17.** Assessment of the asymmetry of commissural involvement and maximum displacement of leaflets according to Nune's scoring system (53). Symmetry denotes commisural area ratio

The new scoring system proposed by Anwar et al. (52) includes a morphologic evaluation of the MV by 3DE with a more detailed anatomical approach. Each scallop is scored separately for calcification, thickness, and mobility as 0 or 1. Importantly, calcifications of A1, A3, P1, and P3 (next to comissures) are given a score of 2 as commissural calcification affects commissural splitting and

Anatol J Cardiol 2020; 23: 128-40
DOI:10.14744/AnatolJCardiol.2020.01575

Kemaloğlu Öz et al.
Multimodality imaging for mitral stenosis

*137*

is a strong predictor of grade >2 mitral regurgitation after PBMC (47, 53). The subvalvular apparatus is also divided into the following three levels: proximal, middle, and distal segments, each being scored for thickness (0, 1) and separation (0, 1, 2). Total 3D score ranges from 0 to 31 points. Mild involvement is scored with <8 points, moderate with 8–13 points, and severe with ≥14 points (52). The strengths of the latter two scoring systems to predict immediate results from PBMC and long-term outcome over Wilkins score relies on the incorporation of commissural morphology and better definition of chordal thickening and fusion, which are best assessed with 3D TOE and clearly underestimated by Wilkins score.

Finally, due to the rapid changes in loading conditions and atrial septal defect immediately following the PBMC, pressure half-time evaluation is prone to errors. 3DE facilitates immediate evaluation of the MVA by planimetry and assessment of commissural splitting, leaflet tears, the site, and degree of new mitral regurgitation in the catheterization laboratory more precisely and accurately than 2DE.

### Multidetector computerized tomography (MDCT)

High resolution of MDCT favors its use as an alternative or complementary method to evaluate the morphological properties of rheumatic MS in patients with poor acoustic windows (54). One can utilize different views of ECG-gated MDCT in contrast to the delineate characteristics of the MV apparatus and to measure the MVA accurately (55). MDCT provides a 3D acquisition of the whole heart and multiplane reconstructions as well; thus, a parasternal short-axis view of the MV orifice at the tips of the leaflets can be obtained for direct planimetric measurement of the MVA (54). A short-axis diastolic view can nicely show the

thickening of the MV leaflets with commissural fusion and calcification. A two-chamber view displays the valve with the characteristic hockey-stick appearance. MDCT is sensitive and can accurately identify calcifications in the leaflets and commissures (56). Moreover, MDCT can show the typical secondary signs of MS including LA enlargement with an anatomically normal left ventricle, pulmonary vein dilatation, pulmonary venous hypertension, and RV dilatation (56). Additionally, MDCT accurately detects thrombus in the LA or LA appendage by late contrast images (Fig. 18). In addition, LA appendage morphology, the angle of the LA appendage bending, and the diameter of the orifice can be accurately measured by MDCT (57).

### Cardiac magnetic resonance

If transthoracic echocardiography is suboptimal or inconclusive and TOE is contraindicated, CMR can be useful. Good demonstration of the restricted MV leaflets can be achieved particularly on the LV outflow tract view. Direct planimetric measurement of the stenotic orifice area by CMR correlates strongly with the pressure half-time method (58). For an accurate measurement of the MVA, the image plane should be positioned at the tips of the MV and multiple parallel thin slices should be taken; otherwise, misalignment may result in significant overestimation (59). CMR also enables visualization of LA appendage morphology and thrombus based on intrinsic tissue characteristics and anatomic appearance. Contrast-enhanced CMR is helpful for assessing thrombus composition and chronicity as a complementary technique to TOE and MDCT (60). Another futuristic approach applied is the phase-contrast imaging to derive velocities, pressure half-time, and definition of the MVA; however, it has to be carefully
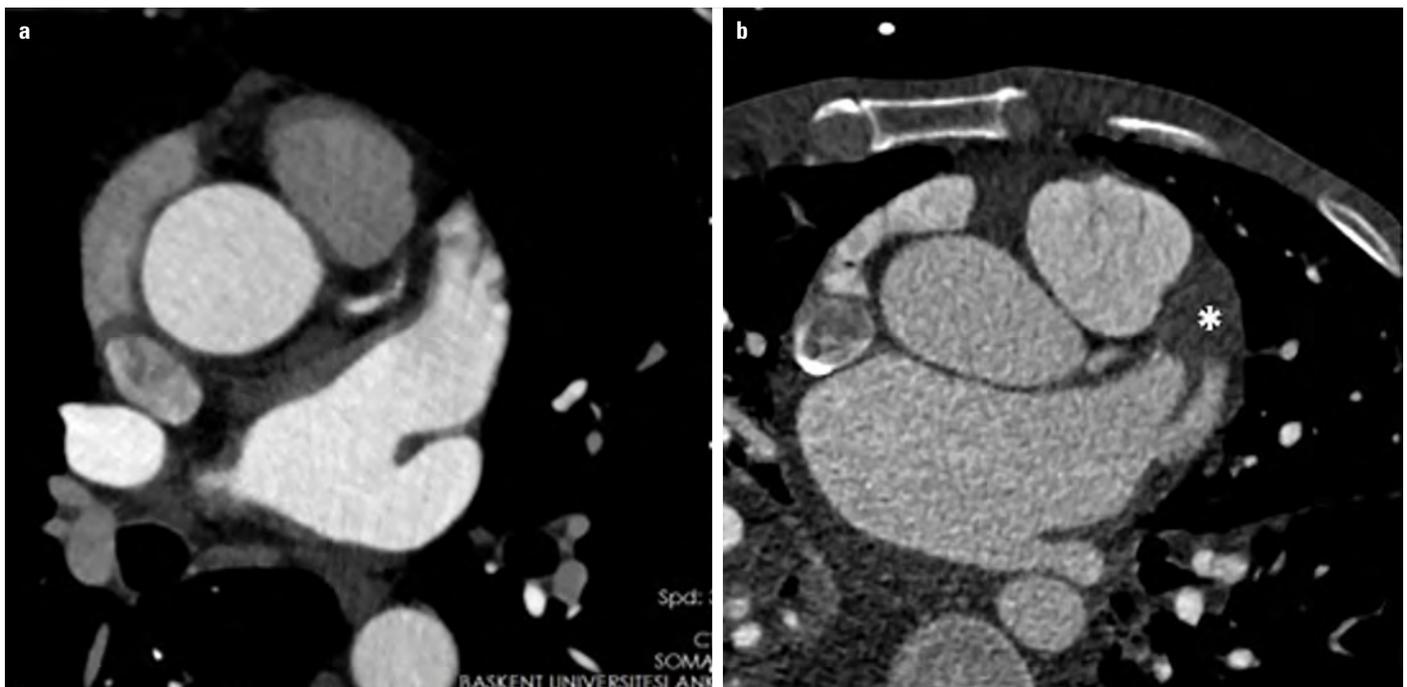
**Figure 18.** LA appendage by MDCT. (a) No thrombus and (b) presence of thrombus within the LA appendage seen on late phase contrast (Asterix) (Courtesy of Dr. Tuncay Hazırolan)
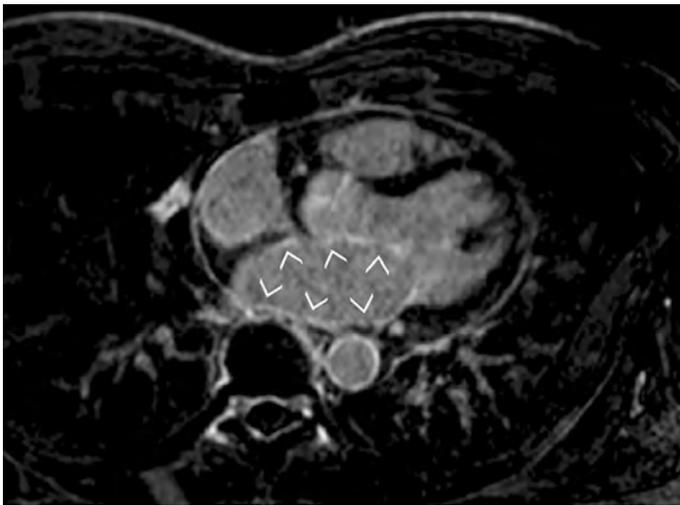
**138** Kemaloğlu Öz et al.
Multimodality imaging for mitral stenosis

Anatol J Cardiol 2020; 23: 128-40
DOI:10.14744/AnatolJCardiol.2020.01575

**Figure 19.** CMR showing enlarged left atrium and fibrosis on the LA wall by late gadolinium hyperenhancement in a patient with mitral stenosis (arrowheads) (Courtesy of Dr. Cemil İzgi)

performed, because low temporal resolution of CMR may cause underestimation of peak velocities (58, 61). RV and LA remodeling is optimally measured by CMR. CMR is also useful for detecting LA fibrosis (Fig. 19) (25). However, CMR remains the third choice if echo and MDCT are inconclusive.

## Conclusion

In conclusion, state of the art approach to the management of patients with rheumatic MS and the new scoring systems requires the use 3DE and multimodality imaging to ensure a thorough assessment of the MV morphology and MS severity. TOE is an integral part of the assessment of rheumatic MS. Stress echocardiography, MDCT, and CMR are complementary tools for the assessment of morphological characteristics of the stenotic MV and their associated structural abnormalities.

**Conflict of interest:** None declared.

**Peer-review:** Internally peer-reviewed.

**Authorship contributions:** Concept – L.E.S.; Design – L.E.S.; Supervision – L.E.S.; Funding – N/A; Materials – N/A; Data collection &/or processing – T.K.Ö., Ö.Ö.T.; Analysis &/or interpretation – T.K.Ö., Ö.Ö.T., L.E.S.; Literature search – T.K.Ö., Ö.Ö.T., L.E.S.; Writing – T.K.Ö., Ö.Ö.T., L.E.S.; Critical review – L.E.S.

## References

1. Nkomo VT, Gardin JM, Skelton TN, Gottdiener JS, Scott CG, Enriquez-Sarano M. Burden of valvular heart diseases: a population-based study. Lancet 2006; 368: 1005-11. [CrossRef]
2. Demirbağ R, Sade LE, Aydın M, Bozkurt A, Acartürk E. The Turkish registry of heart valve disease. Turk Kardiyol Dern Ars 2013; 41: 1-10.
3. Iung B, Baron G, Butchart EG, Delahaye F, Gohlke-Bärwolf C, Levang OW, et al. A prospective survey of patients with valvular heart disease in Europe: the Euro Heart Survey on Valvular Heart Disease. Eur Heart J 2003; 24: 1231-43. [CrossRef]
4. Iung B, Vahanian A. Epidemiology of acquired valvular heart disease. Can J Cardiol 2014; 30: 962-70. [CrossRef]
5. Gujral DM, Lloyd g, Bhattacharyya S. Radiation-induced valvular heart diesae. Heart 2016; 102: 269-76. [CrossRef]
6. Krapf L, Dreyfus J, Cueff C, Lepage L, Brochet E, Vahanian A, et al. Anatomical features of rheumatic and non-rheumatic mitral stenosis: potential additional value of three-dimensional echocardiography. Arch Cardiovasc Dis 2013; 106: 111-5. [CrossRef]
7. Hatle L, Angelsen B, Tromsdal A. Noninvasive assessment of atrioventricular pressure half-time by Doppler ultrasound. Circulation 1979; 60: 1096-104. [CrossRef]
8. Baumgartner H, Hung J, Bermejo J, Chambers JB, Evangelista A, Griffin BP, et al. Echocardiographic assessment of valve stenosis: EAE/ASE recommendations for clinical practice. Eur J Echocardiogr 2009; 10: 1-25. [CrossRef]
9. Rodriguez L, Thomas JD, Monterroso V, Weyman AE, Harrigan P, Mueller LN, et al. Validation of the proximal flow convergence method. Calculation of orifice area in patients with mitral stenosis. Circulation 1993; 88: 1157-65. [CrossRef]
10. Schlosshan D, Aggarwal G, Mathur G, Allan R, Cranney G. Real-time 3D transesophageal echocardiography for the evaluation of rheumatic mitral stenosis. JACC Cardiovasc Imaging 2011; 4: 580-8.
11. Zamorano J, Cordeiro P, Sugeng L, Perez de Isla L, Weinert L, Macaya C, et al. Real-time three-dimensional echocardiography for rheumatic mitral valve stenosis evaluation: an accurate and novel approach. J Am Coll Cardiol 2004; 43: 2091-6. [CrossRef]
12. Min SY, Song JM, Kim YJ, Park HK, Seo MO, Lee MS, et al. Discrepancy between mitral valve areas measured by two-dimensional planimetry and three-dimensional transoesophageal echocardiography in patients with mitral stenosis. Heart 2013; 99: 253-8. [CrossRef]
13. Binder TM, Rosenhek R, Porenta G, Maurer G, Baumgartner H. Improved assessment of mitral valve stenosis by volumetric real-time three-dimensional echocardiography. J Am Coll Cardiol 2000; 36: 1355–61. [CrossRef]
14. Chu JW, Levine RA, Chua S, Poh KK, Morris E, Hua L, et al. Assessing mitral valve area and orifice geometry in calcific MS: A new solution by real-time three-dimensional echocardiography. J Am Soc Echocardiogr 2008; 21: 1006-9. [CrossRef]
15. Nunes MC, Handschumacher MD, Levine RA, Barbosa MM, Carvalho VT, Esteves WA, et al. Role of LA shape in predicting embolic cerebrovascular events in mitral stenosis: mechanistic insights from 3D echocardiography. JACC Cardiovasc Imaging 2014; 7: 453–61. [CrossRef]
16. Overvad TF, Nielsen PB, Larsen TB, Søgaard P. Left atrial size and risk of stroke in patients in sinus rhythm. A systematic review. Thromb Haemost 2016; 116: 206-19. [CrossRef]
17. Nedios S, Koutalas E, Sommer P, Arya A, Rolf S, Husser D, et al. Asymmetrical left atrial remodelling in atrial fibrillation: relation with diastolic dysfunction and long-term ablation outcomes. Europace 2017; 19: 1463-9.
18. Maceira AM, Cosin-Sales J, Roughton M, Prasad SK, Pennell DJ. Reference left atrial dimensions and volumes by steady state free precession cardiovascular magnetic resonance. J Cardiovasc Magn Reson 2010; 12: 65. [CrossRef]
19. Stojanovska J, Cronin P, Patel S, Gross BH, Oral H, Chughtai K, et al. Reference normal absolute and indexed values from ECG-gated

Anatol J Cardiol 2020; 23: 128-40
DOI:10.14744/AnatolJCardiol.2020.01575

Kemaloğlu Öz et al.
Multimodality imaging for mitral stenosis  *139*

MDCT: left atrial volume, function, and diameter. AJR Am J Roentgenol 2011; 197: 631-7. [CrossRef]

20. Mor-Avi V, Yodwut C, Jenkins C, Kühl H, Nesser HJ, Marwick TH, et al. Real-time 3D echocardiographic quantification of left atrial volume: multicenter study for validation with CMR. JACC Cardiovasc Imaging 2012; 5: 769-77. [CrossRef]

21. Miyasaka Y, Tsujimoto S, Maeba H, Yuasa F, Takehana K, Dote K, et al. Left atrial volume by real-time three-dimensional echocardiography: validation by 64-slice multidetector computed tomography. J Am Soc Echocardiogr 2011; 24: 680-6. [CrossRef]

22. Santos AB, Kraigher-Krainer E, Gupta DK, Claggett B, Zile MR, Pieske B, et al.; PARAMOUNT Investigators. Impaired left atrial function in heart failure with preserved ejection fraction. Eur J Heart Fail 2014; 16: 1096-103. [CrossRef]

23. Cameli M, Lisi M, Righini FM, Massoni A, Natali BM, Focardi M, et al. Usefulness of atrial deformation analysis to predict left atrial fibrosis and endocardial thickness in patients undergoing mitral valve operations for severe mitral regurgitation secondary to mitral valve prolapse. Am J Cardiol 2013; 111: 595-601. [CrossRef]

24. Leong DP, Joyce E, Debonnaire P, Katsanos S, Holman ER, Schalij MJ, et al. Left Atrial Dysfunction in the Pathogenesis of Cryptogenic Stroke: Novel Insights from Speckle-Tracking Echocardiography. J Am Soc Echocardiogr 2017; 30: 71-9. [CrossRef]

25. Daccarett M, Badger TJ, Akoum N, Burgon NS, Mahnkopf C, Vergara G, et al. Association of left atrial fibrosis detected by delayed-enhancement magnetic resonance imaging and the risk of stroke in patients with atrial fibrillation. J Am Coll Cardiol 2011; 57: 831-8.

26. Saidi SJ, Motamedi MH. Incidence and factors influencing left atrial clot in patients with mitral stenosis and normal sinus rhythm. Heart 2004; 90: 1342–3. [CrossRef]

27. Wu X, Wang C, Zhang C, Zhang Y, Ding F, Yan J. Computed tomography for detecting left atrial thrombus: a meta-analysis. Arch Med Sci 2012; 8: 943-51. [CrossRef]

28. Dray N, Balaguru D, Pauliks LB. Abnormal left ventricular longitudinal wall motion in rheumatic MS before and after balloon valvuloplasty: a strain rate imaging study. Pediatr Cardiol 2008; 29: 663-6. [CrossRef]

29. Yıldırımtürk Ö, Helvacıoğlu FF, Tayyareci Y, Yurdakul S, Aytekin S. Subclinical left ventricular systolic dysfunction in patients with mild-to-moderate rheumatic mitral stenosis and normal left ventricular ejection fraction: an observational study. Anatol J Cardiol 2013; 13: 328-36.

30. Sengupta SP, Amaki M, Bansal M, Fulwani M, Washimkar S, Hofstra L,et al. Effects of percutaneous balloon mitral valvuloplasty on left ventricular deformation in patients with isolated severe mitral stenosis: a speckle-tracking strain echocardiographic study. J Am Soc Echocardiogr 2014; 27: 639-47. [CrossRef]

31. Fukuda S, Song JM, Gillinov AM, McCarthy PM, Daimon M, Kongsaerepong V, et al. Tricuspid valve tethering predicts residual tricuspid regurgitation after tricuspid annuloplasty. Circulation 2005; 111: 975-9. [CrossRef]

32. Park JB, Lee SP, Lee JH, Yoon YE, Park EA, Kim HK, et al. Quantification of Right Ventricular Volume and Function Using Single-Beat Three-Dimensional Echocardiography: A Validation Study with Cardiac Magnetic Resonance. J Am Soc Echocardipogr 2016; 29: 392-401. [CrossRef]

33. Tanboga IH, Kurt M, Bilen E, Aksakal E, Kaya A, Isik T, et al. Assessment of right ventricular mechanics in patients with mitral stenosis by two-dimensional deformation imaging. Echocardiography 2012; 29: 956-61. [CrossRef]

34. Sade LE, Ozin B, Ulus T, Açikel S, Pirat B, Bilgi M, et al. Right ventricular contractile reserve in mitral stenosis: implications on hemodynamic burden and clinical outcome. Int J Cardiol 2009; 135: 193-201. [CrossRef]

35. Nishimura RA, Otto CM, Bonow RO, Carabello BA, Erwin JP 3rd, Guyton RA, et al.; American College of Cardiology/American Heart Association Task Force on Practice Guidelines. 2014 AHA/ACC guideline for the management of patients with valvular heart disease: executive summary: a report of the American College of Cardiology/American Heart Association Task Force on Practice Guidelines. J Am Coll Cardiol 2014; 63: 2438-88. [CrossRef]

36. Schlosshan D, Aggarwal G, Mathur G, Allan R, Cranney G. Real-time 3D transesophageal echocardiography for the evaluation of rheumatic mitral stenosis. JACC Cardiovasc Imaging 2011; 4: 580-8. [CrossRef]

37. Uygur B, Pusuroglu H, Yildirim A. Percutaneous Mitral Balloon Valvuloplasty in a Pregnant Patient Under Guidance of Three-Dimensional Transesophageal Echocardiography and Right Atrial Mapping, without Using Fluoroscopy. J Heart Valve Dis 2017; 26: 237-9.

38. Eng MH, Salcedo EE, Kim M, Quaife RA, Carroll JD. Implementation of real-time three-dimensional transesophageal echocardiography for mitral balloon valvuloplasty. Catheter Cardiovasc Interv 2013; 82: 994-8. [CrossRef]

39. Schwammenthal E, Vered Z, Agranat O, Kaplinsky E, Rabinowitz B, Feinberg MS. Impact of atrioventricular compliance on pulmonary artery pressure in mitral stenosis: an exercise echocardiographic study. Circulation 2000; 102: 2378-84. [CrossRef]

40. Piérard Luc A, Lancellotti P. Stress testing in valve disease. Heart 2007; 93: 766-72. [CrossRef]

41. Brochet E, Détaint D, Fondard O, Tazi-Mezalek A, Messika-Zeitoun D, Iung B, et al. Early hemodynamic changes versus peak values: what is more useful to predict occurrence of dyspnea during stress echocardiography in patients with asymptomatic mitral stenosis? J Am Soc Echocardiogr 2011; 24: 392-8.

42. Reis G, Motta MS, Barbosa MM, Esteves WA, Souza SF, Bocchi EA. Dobutamine stress echocardiography for noninvasive assessment and risk stratification of patients with rheumatic mitral stenosis. J Am Coll Cardiol 2004; 43: 393-401. [CrossRef]

43. Wilkins GT, Weyman AE, Abascal VM, Block PC, Palacios IF. Percutaneous balloon dilatation of the mitral valve: an analysis of echocardiographic variables related to outcome and the mechanism of dilatation. Br Heart J 1988; 60: 299-308. [CrossRef]

44. Palacios IF, Sanchez PL, Harrell LC, Weyman AE, Block PC. Which patients benefit from percutaneous mitral balloon valvuloplasty? Prevalvuloplasty and postvalvuloplasty variables that predict long-term outcome. Circulation 2002; 105: 1465-71. [CrossRef]

45. Abascal VM, Wilkins GT, O'Shea JP, Choong CY, Palacios IF, Thomas JD, et al. Prediction of successful outcome in 130 patients undergoing percutaneous balloon mitral valvotomy. Circulation 1990; 82: 448-56. [CrossRef]

46. Fatkin D, Roy P, Morgan JJ, Feneley MP. Percutaneous balloon mitral valvotomy with the Inoue single-balloon catheter: commissural morphology as a determinant of outcome. J Am Coll Cardiol 1993; 21: 390-7. [CrossRef]

47. Sutaria N, Shaw TR, Prendergast B, Northridge D. Transoesophageal echocardiographic assessment of mitral valve commissural morphology predicts outcome after balloon mitral valvotomy. Heart 2006; 92: 52-7. [CrossRef]

48. Cannan CR, Nishimura RA, Reeder GS, Ilstrup DR, Larson DR, Holmes DR, et al. Echocardiographic assessment of commissural

**140** Kemaloğlu Öz et al.
Multimodality imaging for mitral stenosis

Anatol J Cardiol 2020; 23: 128-40
DOI:10.14744/AnatolJCardiol.2020.01575

calcium: a simple predictor of outcome after percutaneous mitral balloon valvotomy. J Am Coll Cardiol 1997; 29: 175-80. [CrossRef]

49. Post JR, Feldman T, Isner J, Herrmann HC. Inoue balloon mitral valvotomy in patients with severe valvular and subvalvular deformity. J Am Coll Cardiol 1995; 25: 1129-36. [CrossRef]

50. Iung B, Cormier B, Ducimetiere P, Porte JM, Nallet O, Michel PL, et al. Immediate results of percutaneous mitral commissurotomy. A predictive model on a series of 1514 patients. Circulation 1996; 94: 2124-30. [CrossRef]

51. Nunes MC, Tan TC, Elmariah S, do Lago R, Margey R, Cruz-Gonzalez I, et al. Circulation 2014; 129: 886-95.

52. Anwar AM, Attia WM, Nosir YF, Soliman OI, Mosad MA, Othman M, et al. Validation of a new score for the assessment of MS using real-time three-dimensional echocardiography. J Am Soc Echocardiogr 2010; 23: 13-22. [CrossRef]

53. Messika-Zeitoun D, Blanc J, Iung B,Brochet E, Cormier B, Himbert D, et al. Impact of degree of commissural opening after percutaneous mitral commissurotomy on long-term outcome. JACC Cardiovasc Imaging 2009; 2: 1-7. [CrossRef]

54. Messika-Zeitoun D, Serfaty JM, Laissy JP, Berhili M, Brochet E, Iung B, et al. Assessment of the mitral valve area in patients with mitral stenosis by multislice computed tomography. J Am Coll Cardiol 2006; 48: 411-3. [CrossRef]

55. Willmann JK, Kobza R, Roos JE, Lachat M, Jenni R, Hilfiker PR, et al. ECG-gated multi-detector row CT for assessment of mitral valve disease: initial experience. Eur Radiol 2002; 12: 2662-9. [CrossRef]

56. Chheda SV, Srichai MB, Donnino R, Kim DC, Lim RP, Jacobs JE. Evaluation of the mitral and aortic valves with cardiac CT angiography. J Thorac Imaging 2010; 25: 76-85. [CrossRef]

57. Santangeli P, Di Biase L, Horton R, Burkhardt D, Natale A. CT Imaging to Assess the Left Atrial Appendage Anatomy: Clinical Implications. In: Saba L, editor. Computed Tomography-Clinical Applications. InTech; 2012. p.241-52.

58. Helvacioglu F, Yıldırımtürk O, Duran C, Yurdakul S, Tayyareci Y, Ulusoy OL, et al. The evaluation of mitral valve stenosis: comparison of transthoracic echocardiography and cardiac magnetic resonance. Eur Heart J Cardiovasc Imaging 2014; 15: 164-9. [CrossRef]

59. Myerson SG. Heart valve disease: investigation by cardiovascular magnetic resonance. J Cardiovasc Magn Reson 2012; 14: 7. [CrossRef]

60. Goyal P, Weinsaft JW. Cardiovascular magnetic resonance imaging for assessment of cardiac thrombus. Methodist Debakey Cardiovasc J 2013; 9: 132-6. [CrossRef]

61. Lin SJ, Brown PA, Watkins MP, Williams TA, Lehr KA, Liu W, et al. Quantification of stenotic mitral valve area with magnetic resonance imaging and comparison with Doppler ultrasound. J Am Coll Cardiol 2004; 44: 133-7. [CrossRef]